Available online at www.sciencedirect.com
SCIENCE DIRECT®
Journal of Sound and Vibration 283 (2005) 311–339
JOURNAL OF SOUND AND VIBRATION
www.elsevier.com/locate/jsvi

Adaptive active control of flexible structures subjected to rigid body displacements

L. Gaudiller[a,*], S. Bochard[b]

[a] *Laboratoire de Dynamique des Machines et des Structures, UMR 5006 CNRS, Institut National des Sciences Appliquées, Bâtiment d'Alembert, 8 rue des Sciences, 69621 Villeurbanne, France*
[b] *Université de Bretagne Sud, 2 rue le Coat St Haouen, BP 92116, 56321 Lorient Cedex, France*

Received 23 September 2003; accepted 14 April 2004
Available online 10 December 2004

Abstract

When flexible structures are subjected to rigid body displacements, their dynamic behavior presents a coupling between rigid body displacements and flexible modes. Moreover, if these structures are articulated, their inertia characteristics can vary considerably through time and cause this dynamic behavior to become highly nonlinear.

The paper presents the principle of a new adaptive controller MIMO. making it possible to render nearly constant the dynamic behavior of multi-articulated flexible structures in spite of changes in the geometry of their masses. The principle of this controller is based on the operation in parallel of a number of finite Gaussian quadratic linear controllers calculated before simulations, for the operating points crossed during the motion. The global multivariable command generated by the adaptive controller is the sum of the commands generated by the linear controllers, weighted by functions of rigid body displacements to allow the smoothing of the control actions on the structure.

Adaptive control is first applied to a rigid bi-articulated structure, then to mono-articulated and bi-articulated flexible structures equipped with piezoelectric sensors and piezoelectric and electromechanical actuators. After temporal optimization, the results of the proposed adaptive control are compared with those of a linear controller. This is done by using two methods, chosen according to whether the structures are stressed by disturbances or by tracking.

In the case of regulation, the performances of this controller highlight on the one hand, the near-constant dynamic behavior of the controlled structure by eliminating instabilities, in spite of the considerable changes of kinetics and, on the other hand, clearly improved performances when compared to a fixed linear

*Corresponding author. Tel.: +33-472-438-823; fax: +33-472-438-930.
E-mail address: luc.gaudiller@insa-lyon.fr (L. Gaudiller).

0022-460X/$ - see front matter
doi:10.1016/j.jsv.2004.04.039

controller. In the case of a set point tracking, performances in terms of rapidity are also appreciably improved compared to those of a linear controller, while guaranteeing stability, significant damping and absolute precision without residual strains when the commands are performed.

1. Introduction

The potential applications of the active control of flexible structures subjected to rigid body displacements are numerous and varied. For example, in the field of robotics, fast rotations of articulated arms cause vibratory behavior of the structure incompatible with the precision requirements at the end of arm obtained by classical controllers. In the space engineering field, the deployment of very flexible solar panels produces significant dynamic though non-damped deformations, which considerably influence the orientation of satellites. The dynamic behavior of mechanisms with on-board flexible rotors used in the field of transportation can be greatly disturbed by vehicle kinematics. These ever more efficient structures, whose dynamic behavior is often nonlinear, now require active control. Linear controllers [1] are often ineffective or unsuited because of the structure's nonlinear behavior and mechanical couplings: rigid body displacements/vibration are significant and generate instabilities.

Several approaches have been developed to simulate these couplings in the framework of flexible multi-articulated structures. The nonlinear motion equations of the flexible structure subjected to rigid body displacements can be obtained in analytical form by Lagrange equations. The flexible parts are then approximated by Timoshenko beams [2] or modal forms [3,4] with a possible explicit formulation in the case of the beams [5]. The use of these methods for complex structures is difficult. In this case, discretization of geometry by the finite element (FE) method is adapted [6], but the computer memory capacities required and the computing times are significant. To reduce them a modal projection adapted to dynamics is employed [7].

The simulation of the coupling between rigid body displacements and vibrations makes it possible to adjust the controllers precisely and test the proposed control strategies correctly. For this type of structure, the control methods proposed do not often take these couplings and their consequences on global feedback into account. Generally, several controllers are used to process the solid modes and the flexible modes [8,9] independently. They disturb each other via the mechanical coupling between vibrations/rigid body displacements on the one hand, and between flexible modes on the other hand. The control performances obtained are low because the gains of the controller must be limited to maintain stability or else it must be guaranteed by weak coupling. The robustness of stability is thus appreciably affected. In order to guarantee it, algorithms of type $H\infty$, LTR or of type "Quantitative Theory Feedback" can be used [10–12] but the performances of these controllers remain non-optimal.

The multivariable controllers can take into account the mechanical couplings [10–13], which make it possible to minimize the corresponding disturbances. In this case, the control gains can be optimized by using quadratic linear algorithms with an energy performance criterion. In the case of the flexible structures, the projection of physical displacements on a modal basis allows the observation and the control of each mode by independent sensors and actuators [14], whose

number can be reduced by using an observer and control set [1]. However, projection in modal space, then modal reduction in the observation and control bands, leads to a risk of instability of the non-controlled modes: spillover [15].

The main problems in implementing the control of flexible structures are: spillover and adjustment of the band-width of the controllers and actuators. In the case of a multivariable controller, the first two problems can be reduced significantly if the model is accurate [11,13], the control band-width is significant, and that the controller is robust. This method was illustrated by experimental works [9,16] in the case of SIMO systems. In addition to the actuators generating rigid body displacements, the piezoelectric actuators make it possible to widen the control band-width. Many works have been carried out using ceramics in the same way as sensors [9] or actuators [17,18]. They are used since they are easy to incorporate in the structures owing to their lightness, compactness and especially the distribution of efforts and strains due to control, causing the reduction of the corresponding spillover. Pairs of colocalized actuators–sensors, with wide band-widths are available and usable today [19,20]. Their integration in flexible structures was initially studied analytically by integrating simplified local relations, where piezoelectric ceramics was modeled on the basis of uniform stress field [21] and linear [22–24] hypotheses. The transfer functions of the transducers used characterize the voltage–torque or loading–bending relations [21], then, an FE approach allowed the elimination of the limitations created by the previous assumptions by discretizing any geometry of the structure/piezoelectric components assembly [25]. The complete local relations of the piezoelectric material are directly integrated and translated by structural and electric matrices [26].

In this paper, an adaptive control strategy is developed to control the strongly nonlinear dynamic behavior of a bi-articulated flexible structure with couplings between rigid body displacements and vibrations, by using piezoelectric patches and electric motors. The adaptive control consists in weighting the command of the controllers operating in parallel, and calculated for the operating points crossed during the motion. The multivariable command (MIMO) is obtained by interpolating the linear quadratic command of each controller optimized according to rigid body displacements.

2. Adaptive controller design

The dynamic behavior of multi-articulated structures has strong nonlinearities, primarily due to the modification of their geometrical configuration during motion. For example, in the case of the bi-articulated structure schematized in Fig. 1, the strongly nonlinear behavior is induced by the modification of its moment of inertia around $(A, \mathbf{z}_0)$ during the rotation of the flexible beam 2.

Consequently, a linear control, formulated from a linear model, is not adapted when the structure moves away from the point of linearization that permitted calculating the controller: the more the structure moves away from this point, the more the performance and robustness of the control degrade until instability. It is therefore necessary to guarantee the stability and improve the performance of the control by taking the geometrical modification of the structure into account.

In addition, the vibrations of beam 2 are coupled with the displacements of rigid bar 1 and with the rotation of its own rigid body. Control must therefore be global in order to maximize

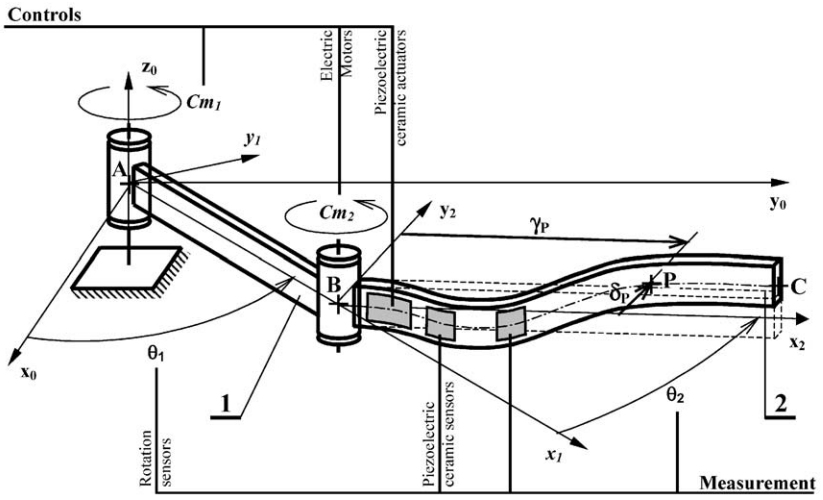

Fig. 1. Bi-articulated flexible structure configuration and parameters.

performance and minimize spillover between the rigid and flexible modes. A global linear control of a linear structure, based on a LQG type algorithm provides good performances [1] and robustness provided that it is formulated on the basis of an accurate model of the structure to be controlled.

The control strategy proposed, presented in Fig. 2, uses a finite number of these linear controllers. They are built for a finite number of operating points crossed during the motion of the structure and they operate in parallel. When the structure is between two operating points, the controllers of the closest operating points are selected so that their respective commands participate in the command transmitted to the actuators.

The linear controllers are calculated on the basis of the model of the structure's nonlinear dynamic behavior. This is linearized around each one of the operating points p chosen among those crossed when the structure is in motion. The state form obtained for the ith operating point is written as

$$\dot{\mathbf{x}} = \mathbf{A}_i\mathbf{x} + \mathbf{B}_i\mathbf{u}_i \tag{1}$$

with $\mathbf{x}$, as the state vector of the structure including n_x states, made up of rigid body displacements, corresponding speeds, modal displacements $\mathbf{q}_j$ and modal speeds $\dot{\mathbf{q}}_j$ of the structure reduced to n first modes to be controlled

$$\mathbf{x} = [\boldsymbol{\theta}\ \mathbf{q}\ \dot{\boldsymbol{\theta}}\ \dot{\mathbf{q}}]^{\mathrm{t}} \tag{2}$$

and $\mathbf{u}_i$ as the control vector of the ith controller, $\mathbf{A}_i$ and $\mathbf{B}_i$ being the respective matrices of the structure's dynamics and of the control at the ith operating point.

Once the gains matrices $\mathbf{G}_i$ of the linear controllers have been calculated, the vector $\mathbf{u}$ of the global state feedback command of the structure is calculated by weighting the commands of the linear controllers of the closest operating points. Indeed, the participation of the selected linear commands must guarantee the continuity of the global command, while ensuring the passage

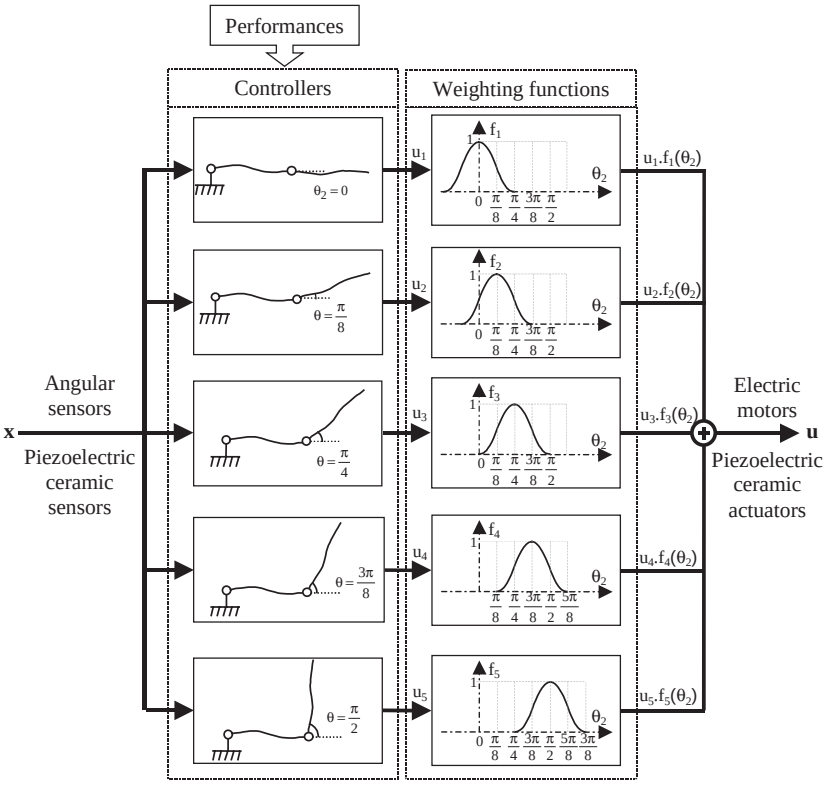

Fig. 2. Principle of the adaptive controller.

from one controller to another. To do this, weighting functions f_i (see Fig. 1), which are functions of rigid body displacements $\boldsymbol{\theta}$, are used for each linear controller command. Thus, starting from the p operating points crossed by the structure, vector $\mathbf{u}$ of the global command is thus written as follows:

$$\mathbf{u} = \sum_{i=1}^{p} f_i(\boldsymbol{\theta})\mathbf{G}_i\mathbf{x} = \mathbf{G}(\boldsymbol{\theta})\mathbf{x}. \tag{3}$$

In order to guarantee the progressive evolution of the global command, the sum of the weight functions is fixed at 1. General stability is thus ensured over the entire operating range while the modulation of the dynamics of nonlinear control is a function of the number of operating points.

In the case of the bi-articulated flexible structure presented in Fig. 1, θ_2 is the rigid body displacement parameter that governs the geometrical modifications of the model of the structure. When the motion of the structure is such that θ_2 moves between $-\pi/2$ and $\pi/2$, the nonlinear terms change considerably. The corresponding nonlinear controller is presented in Fig. 2 for sector $(0, \pi/2)$ when nine linearization points are selected, symmetrical compared to 0 as

$$[-\pi/2,\ -3\pi/8,\ -\pi/4,\ -\pi/8,\ 0,\ \pi/8,\ \pi/4,\ 3\pi/8,\ \pi/2]. \tag{4}$$

It will have the following form for the nine of linearization points:

$$\mathbf{u} = \sum_{i=1}^{9} f_i(\theta_2)\mathbf{G}_i\mathbf{x} = \mathbf{G}(\theta_2)\mathbf{x}. \tag{5}$$

In the case of these bi-articulated structures, the selected interpolation functions f_i are simple limited linear interpolations. Fig. 3 presents the action fields of each controller induced by the linear interpolation functions.

For each linear controller, it is necessary to ensure the static precision of the control of rigid body displacements $\boldsymbol{\theta}$ generated by the torques $\mathbf{C}_m$.This is carried out, on the one hand, by adding the integral of the error between the displacements and the corresponding set points to the state vector of the system and, on the other hand, by adding the voltages $\mathbf{V}_a$ of the actuators controlling the flexible modes. These voltages are forced to zero, by integration, to obtain a null curvature of the structure when the static position is reached. The corresponding outputs $\mathbf{Y}_c$ necessary to create these integral states are obtained on the basis of the state of the system and the command of the general controller **u,** controlling the n_u actuators, and weighting each

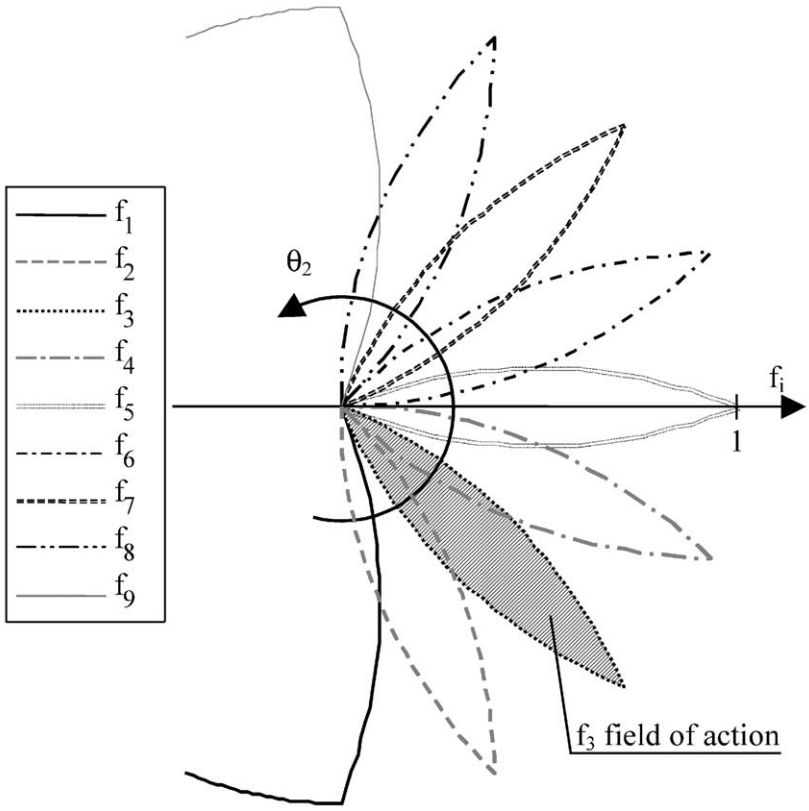

Fig. 3. Field of action of each linear controller induced by f_i functions of linear interpolation.

command $\mathbf{u}_i$:

$$\mathbf{y}_c = \begin{Bmatrix} \boldsymbol{\theta} \\ \mathbf{v}_a \end{Bmatrix} = \mathbf{C}_c\mathbf{x} + \mathbf{D}_c\mathbf{u} = \begin{bmatrix} \mathbf{I} & \mathbf{0} & \mathbf{0} & \mathbf{0} \\ \mathbf{0} & \mathbf{0} & \mathbf{0} & \mathbf{0} \end{bmatrix} \begin{Bmatrix} \boldsymbol{\theta} \\ \mathbf{q} \\ \dot{\boldsymbol{\theta}} \\ \dot{\mathbf{q}} \end{Bmatrix} + \begin{bmatrix} \mathbf{0} & \mathbf{0} \\ \mathbf{0} & \mathbf{I} \end{bmatrix} \begin{Bmatrix} \mathbf{C}_m \\ \mathbf{v}_a \end{Bmatrix}. \tag{6}$$

The state system $\dot{\mathbf{x}}_a$ augmented by n_c state variables necessary for the static precision without curvature is therefore written as

$$\dot{\mathbf{x}}_a = \begin{Bmatrix} \dot{\mathbf{x}} \\ \dot{\mathbf{p}} \end{Bmatrix} = \mathbf{A}_{ai}\mathbf{x}_a + \mathbf{B}_{ai}\mathbf{u} + \mathbf{B}_z\mathbf{z} = \begin{bmatrix} \mathbf{A}_i & \mathbf{0} \\ \mathbf{C}_c & \mathbf{0} \end{bmatrix} \begin{Bmatrix} \mathbf{x} \\ \mathbf{p} \end{Bmatrix} + \begin{bmatrix} \mathbf{B}_i \\ \mathbf{D}_c \end{bmatrix} \mathbf{u} + \begin{bmatrix} \mathbf{0} \\ \mathbf{I} \end{bmatrix} \mathbf{z} \tag{7}$$

with the integral $\mathbf{p}$ of the potential correction vector $\boldsymbol{\varepsilon}$:

$$\mathbf{p} = \int_0^{\mathrm{t}} \boldsymbol{\varepsilon}\, \mathrm{d}t, \qquad \boldsymbol{\varepsilon} = \mathbf{y}_c - \mathbf{z}, \qquad \mathbf{z} = \begin{Bmatrix} \boldsymbol{\theta} & \boldsymbol{\theta}_c \\ \mathbf{v}_a & \mathbf{0} \end{Bmatrix}. \tag{8}$$

Since the linear controllers are subjected to stress around their own operating points, their robustness decreases by as much as the number p of operating points is small. A linear quadratic (LQ) type algorithm is selected for its robustness once the model is readjusted accurately. Adjustment of performances and power consumption is carried out by the weightings $\mathbf{Q}_i$ and $\mathbf{R}_i$ of the performance index J_i

$$J_i = \frac{1}{2}\int_0^{\infty} (\mathbf{x}_a^{\mathrm{t}}\mathbf{Q}_i\mathbf{x}_a + \mathbf{u}_i^{\mathrm{t}}\mathbf{R}_i\mathbf{u}_i)\, \mathrm{d}t \tag{9}$$

with each command $\mathbf{u}_i$ of linear controllers being written as

$$\mathbf{u}_i = -G'_{\boldsymbol{i}} - \mathbf{x}_a = -\mathbf{R}^{-1}\, \mathbf{B}_{ai}^{\mathrm{T}}\, \mathbf{S}_i\mathbf{x}_a \tag{10}$$

with the $\mathbf{G}_i$ gain matrices obtained by the minimization of index (9), at an infinite control horizon, which is carried out by obtaining Riccati matrix $\mathbf{S}$, from the algebraic equation

$$\mathbf{S}_i\, \mathbf{A}_{ai} + \mathbf{A}_{ai}^{\mathrm{t}}\mathbf{S}_i + \mathbf{S}_i\, \mathbf{B}_{ai}\mathbf{R}^{-1}\mathbf{B}_{ai}^{\mathrm{t}}\mathbf{S}_i - \mathbf{Q} = \mathbf{0} \tag{11}$$

the linear commands obtained makes it possible to minimize performance losses caused by the necessarily reduced number of actuators compared to the number of modes to be controlled [1].

If the model of the structure to be controlled is complex, it is then necessary to optimize the coefficients of weighting matrices $\mathbf{Q}_i$ and $\mathbf{R}_i$ of the LQ controller used in the calculation of the gains $\mathbf{G}_x$. In this study, the principle of selected optimization is based on the comparison between the responses and the simulated commands, with temporal templates subjected to gradual constraints. This method has the advantage of using physical knowledge of the behavior of the structure controlled to create the templates, while generating stable control.

The temporal optimization algorithm proceeds by iteration, adjusting the weightings of performance $\mathbf{Q}_i$ and $\mathbf{R}_i$ until obtaining a controlled response corresponding to the fixed templates.

To carry out this optimization, the following $n_x+n_c+n_u$ variables $\mathbf{v}_i$, corresponding to the coefficients of matrices $\mathbf{Q}$ and $\mathbf{R}$, are used as design variables

$$\mathbf{Q} = \text{diag}\,[\mathbf{v}_i] \quad \text{with } i \in [1, n_x + n_c], \tag{12}$$

$$\mathbf{R} = \text{diag}\,[\mathbf{v}_i] \quad \text{with } i \in [n_x + n_c + 1, n_x + n_c + n_u]. \tag{13}$$

After having collected these variables in a vector $\mathbf{v}$ and limited their variation by

$$\mathbf{v}_{\text{inf}} < \mathbf{v} < \mathbf{v}_{\text{sup}}. \tag{14}$$

For each iteration, temporal responses are simulated by the control loop on N_P discretized points. The responses are then compared with the temporal templates (Fig. 11). These comparisons make it possible to calculate the constraint vector $\mathbf{g}(\mathbf{v})$ containing the difference of the responses between the calculated points of the optimized temporal curves and the high and low bounds of the templates. Thus the optimization problem is reduced to

$$\min_{v} \ \lambda / \begin{vmatrix} \mathbf{g}(\mathbf{v}) - \mathbf{w}\lambda \leqslant 0 \\ \mathbf{v}_{\text{inf}} < \mathbf{v} < \mathbf{v}_{\text{sup}} \end{vmatrix} \tag{15}$$

with $\mathbf{w}$ being the constraints weighting vector and λ, a positive scalar which imposes maximal conformity of the constraints while tending towards zero. When this optimization is carried out, $\mathbf{w}$ is updated while assigning a weight to each constraint, which is as great as its degree of violation. When the progression of the constraints and the optimization variables exceeds a threshold defined in a convergence criterion, the optimization ends by corresponding to a local minimum.

3. Modeling of instrumented bi-articulated flexible structures

The bi-articulated structure concerned by the study is drawn and parameterized in Fig. 1. The vibrations of beam 2 are coupled with rigid body displacements of rigid bar 1 and with its own overall rotation. The structure has strongly nonlinear behavior caused by the modification of its moment of inertia around $(A, \mathbf{z}_0)$ during the rotation of beam 2. Bar 1 has mass m_1, length, L_1 and inertia I_1 in A. It turns at angle θ_1 around A due to engine torque. C_{ml}. The monodimensional rectilinear flexible beam 2, has mass m_2, length L_2, and inertia I_2 in B. It turns at angle θ_2 around B due to engine torque. Its neutral line, controlled and observed by piezoelectric patches is modeled by all the material points P, mass, m_p, X coordinate γ_p on $(B, \mathbf{x}_2)$, and transverse displacement δ_p. The motions are carried out in the horizontal plane $(\text{O}, \mathbf{x}_0, \mathbf{y}_0)$. Since gravity is exerted according to the downward vertical, it does not influence the motion.

The quality of adaptive multivariable control depends on quality of the model. Thus the following model incorporates, rigid body displacements/vibrations couplings, the non-linearities induced by rigid body and flexible displacements, and the coupling piezoelectric effects/structure. It will be fitted optimally further on.

The kinetic energy T of the bi-articulated structure is given by

$$T = \tfrac{1}{2} I_1 \dot{\theta}_1^2 + \tfrac{1}{2} \int_0^{L_2} m_p \dot{r}_p^2 \, \mathrm{d}\gamma_p \tag{16}$$

with r_p being the position of the point P in the fixed base, which can be expressed based on modal participations q_j established on the associated conservative basis Φ_p of the n first modes of the beam, such as

$$\dot{r}_P^2 = L_1^2\dot{\theta}_1^2 + \mathbf{q}^t\mathbf{\Phi}_P^t\mathbf{\Phi}_P\mathbf{q}(\dot{\theta}_1+\dot{\theta}_2)^2 + \gamma_P^2(\dot{\theta}_1+\dot{\theta}_2)^2 + \dot{\mathbf{q}}^t\mathbf{\Phi}_P^t\mathbf{\Phi}_P\dot{\mathbf{q}} - 2L_1\mathbf{\Phi}_P^t\mathbf{q}\dot{\theta}_1(\dot{\theta}_1+\dot{\theta}_2)\sin\,\theta_2 + 2\gamma_P\mathbf{\Phi}_P^t\dot{\mathbf{q}}(\dot{\theta}_1+\dot{\theta}_2) + 2L_1\gamma_P\mathbf{q}\dot{\theta}_1(\dot{\theta}_1+\dot{\theta}_2)\cos\,\theta_2 + 2L_1\mathbf{\Phi}_P^t\dot{\mathbf{q}}\dot{\theta}_1\,\cos\,\theta_2. \tag{17}$$

The equations of behavior of beam 2 provided by the actuators and piezoelectric sensors are written as

$$\begin{Bmatrix}\boldsymbol{\sigma}\\ \mathbf{d}\end{Bmatrix} = \begin{bmatrix}\mathbf{Y} & \mathbf{Z}\\ \mathbf{Z}^t & -\mathbf{\Sigma}\end{bmatrix}\begin{Bmatrix}\mathbf{s}\\ -\mathbf{e}\end{Bmatrix} \tag{18}$$

with $\boldsymbol{\sigma}$ being the vector of the constraints, $\mathbf{d}$ the intensity vector, $\mathbf{Y}$ the matrix of elasticity with a constant electric field, $\mathbf{Z}$ the piezoelectric matrix, $\mathbf{\Sigma}$ the matrix of permittivity evaluated at constant deformation, $\mathbf{s}$ the strain vector, and $\mathbf{e}$ the electric field, which can be expressed by the terminal voltages of the ceramics via matrix $\mathbf{Q}$:

$$\mathbf{s} = \mathbf{Q}\mathbf{v}. \tag{19}$$

Sum $\mathscr{P}^*$ of the virtual mechanical powers and internal electric powers of instrumented beam 2 is obtained from (18), and the external electric power of the current supply of ceramics is obtained by vector $\mathbf{q}_e$ acting on the vector of the virtual voltage variations, $\dot{\mathbf{v}}^*$, and the external power of the electric motors delivering the respective couples C_{m_1} and C_{m_2}. By carrying out the modal projection of the strain by using matrix $\mathbf{H}$, it can be written as

$$\mathscr{P}^* = -\dot{\mathbf{q}}^{t*}\left[\int_{P\in S_2}\mathbf{H}^t\mathbf{Y}\mathbf{H}\,\mathrm{d}\otimes(P)\right]\mathbf{q} + \dot{\mathbf{q}}^{t*}\left[\int_{P\in S_2}\mathbf{H}^t\mathbf{Z}\mathbf{Q}\,\mathrm{d}\otimes(P)\right]\mathbf{v} + \mathbf{v}'^*\left[\int_{P\in S_2}\mathbf{Q}^t\mathbf{Z}^t\mathbf{H}\,\mathrm{d}\otimes(P)\right]\mathbf{q} + \mathbf{v}^{t*}\left[\int_{P\in S_2}\mathbf{Q}^t\mathbf{\Sigma}\mathbf{Q}\,\mathrm{d}\otimes(P)\right]\mathbf{v} + \mathbf{v}^{t*}\mathbf{q}_e^t + C_{m_1}\dot{\theta}_1^* + C_{m_2}\dot{\theta}_2^*. \tag{20}$$

When the structure is discretized by finite elements, a Guyan condensation on N_R main nodes along the beam makes it possible to establish the link between the wired analytical model and the discretized model, even in the event of 3D meshing. An interpolation using the matrix N_p makes it possible to obtain the following relation:

$$\gamma_p = \mathbf{N}_p\boldsymbol{\gamma};\quad \boldsymbol{\delta}_p = \mathbf{N}_p\boldsymbol{\delta};\quad \mathbf{\Phi}_p = \mathbf{N}_p\mathbf{\Phi}. \tag{21}$$

Likewise, an interpolation of the discrete modal base using matrix $\mathbf{B}_s$ makes it possible to obtain the link between continuous and discrete models for the strains starting from transverse displacements $\boldsymbol{\delta}$

$$\mathbf{s} = \mathbf{B}_s\boldsymbol{\delta};\quad \mathbf{H} = \mathbf{B}_s\mathbf{\Phi}. \tag{22}$$

Thus the kinetic energy and the total virtual power of the discretized structure are

$$T = \tfrac{1}{2}(I_1+m_2L_1^2)\dot{\theta}_1^2 + \tfrac{1}{2}(I_2+\mathbf{q}^t\mathbf{q})(\dot{\theta}_1+\dot{\theta}_2)^2 + \tfrac{1}{2}\dot{\mathbf{q}}^t\dot{\mathbf{q}} + \boldsymbol{\gamma}^t\mathbf{M}\mathbf{\Phi}\dot{\mathbf{q}}(\dot{\theta}_1+\dot{\theta}_2) + L_1^t\mathbf{M}\mathbf{\Phi}\dot{\mathbf{q}}\dot{\theta}_1\,cos\,\theta_2 + L_1^t\mathbf{M}(\boldsymbol{\gamma}\,\cos\,\theta_2 - \phi q\,\sin\,\theta_2)\dot{\theta}_1(\dot{\theta}_1+\dot{\theta}_2), \tag{23}$$

$$\mathscr{P}^* = -\dot{\mathbf{q}}^{*\mathrm{t}}\mathbf{\Phi}^{\mathrm{t}}\mathbf{K}\mathbf{\Phi}\mathbf{q} + \dot{\mathbf{q}}^{*\mathrm{t}}\mathbf{\Phi}^{\mathrm{t}}\mathbf{\Pi}\mathbf{v} + \dot{\mathbf{v}}^{*\mathrm{t}}\mathbf{\Pi}^{\mathrm{t}}\mathbf{\Phi}\mathbf{q} + \dot{\mathbf{v}}^{*\mathrm{t}}\mathbf{\Lambda}\mathbf{v} + \dot{\mathbf{v}}^{*\mathrm{t}}\mathbf{q}_{\mathrm{e}}^{\mathrm{t}} + C_{m_1}\dot{\theta}_1^* + C_{m_2}\dot{\theta}_2^* \tag{24}$$

with

$$\mathbf{K} = \int_{P\in S_2} \mathbf{B}_s^{\mathrm{t}}\mathbf{Y}\mathbf{B}_s \,\mathrm{d}\tau(P), \tag{25}$$

$$\mathbf{M} = \int_0^{L_2} m_p \mathbf{N}_p^{\mathrm{t}}\mathbf{N}_p \,\mathrm{d}\gamma_p, \tag{26}$$

$$\mathbf{\Pi} = \int_{P\in S_2} \mathbf{B}_s^{\mathrm{t}}\mathbf{Z}\mathbf{Q} \,\mathrm{d}\tau(P), \tag{27}$$

$$\mathbf{\Lambda} = \int_{P\in S} \mathbf{Q}^{\mathrm{t}}\mathbf{\Sigma}\mathbf{Q} \,\mathrm{d}\tau(P). \tag{28}$$

The Lagrange equations are written on the basis of expressions (23) and (24). Then, since the structure is assumed to be slightly damped, with uncoupled modes, damping is introduced via the diagonal modal matrix $\mathscr{C}$. The motion equations, including the vibration/rigid body displacement coupling, of the dynamic behavior of the instrumented bi-articulated structure are then obtained as

$$\ddot{\theta}_1 = [(I_{22} - I_{2q}I_{q2})(C_1 - I_{1q}\mathbf{C}_q) - (I_{12} - I_{1q}I_{q2})(C_2 - I_{2q}\mathbf{C}_q)]/D, \tag{29}$$

$$\ddot{\theta}_2 = [-(I_{12} - I_{2q}I_{q1})(C_1 - I_{1q}\mathbf{C}_q) + (I_{11} - I_{1q}I_{q1})(C_2 - I_{2q}\mathbf{C}_q)]/D, \tag{30}$$

$$\begin{aligned}\ddot{\mathbf{q}} = \mathbf{C}_q &- I_{q1}[(I_{22} - I_{2q}I_{q2})(C_1 - I_{1q}\mathbf{C}_q) - (I_{12} - I_{1q}I_{q2})(C_2 - I_{2q}\mathbf{C}_q)]/D \\ &+ I_{q2}[(I_{12} - I_{2q}I_{q1})(C_1 - I_{1q}\mathbf{C}_q) - (I_{11} - I_{1q}I_{q1})(C_2 - I_{2q}\mathbf{C}_q)]/D\end{aligned} \tag{31}$$

with

$$I_{11} = I_1 + I_2 + \mathrm{m}_2 L_1^2 + \mathbf{q}^{\mathrm{t}}\mathbf{q} + 2\mathscr{L}_1^{\mathrm{t}}\mathbf{M}(\boldsymbol{\gamma}\ \cos\ \theta_2 - \mathbf{\Phi}\mathbf{q}\ \sin\ \theta_2), \tag{32}$$

$$I_{12} = I_{21} = I_2 + \mathbf{q}^{\mathrm{t}}\mathbf{q} + \mathscr{L}_1^{t}\mathbf{M}(\boldsymbol{\gamma}\cos\ \theta_2 - \mathbf{\Phi}\mathbf{q}\ \sin\ \theta_2), \tag{33}$$

$$I_{1q} = I_{q1} = \boldsymbol{\gamma}^{\mathrm{t}}\mathbf{M}\mathbf{\Phi} + \mathscr{L}_1^{\mathrm{t}}\mathbf{M}\mathbf{\Phi}\ \cos\ \theta_2, \tag{34}$$

$$I_{q2} = I_{2q}^{\mathrm{t}} = \mathbf{\Phi}^{\mathrm{t}}\mathbf{M}\gamma, \tag{35}$$

$$I_{22} = I_2 + \mathbf{q}^{\mathrm{t}}\mathbf{q}, \tag{36}$$

$$C_1 = C_{m_1} + (2\dot{\theta}_1 + \dot{\theta}_2)\dot{\theta}_2\mathscr{L}_1^{\mathrm{t}}\mathbf{M}(\cos\ \theta_2\mathbf{\Phi}\mathbf{q} + \sin\ \theta_2\boldsymbol{\gamma}) - 2(\dot{\theta}_1 + \dot{\theta}_2)(\mathbf{q}^{\mathrm{t}} - \sin\theta_2\mathscr{L}_1^{\mathrm{t}}\mathbf{M}\mathbf{\Phi})\dot{\mathbf{q}}, \tag{37}$$

$$C_2 = C_{m_2} - \dot{\theta}_1^2 L_1^{\mathrm{t}}\mathbf{M}(\cos\ \theta_2\ \mathbf{\Phi}\mathbf{q} + \sin\ \theta_2\ \boldsymbol{\gamma}) - 2(\dot{\theta}_1 + \dot{\theta}_2)\mathbf{q}^{\mathrm{t}}\dot{\mathbf{q}}, \tag{38}$$

$$C_q = \mathscr{A}\mathbf{v} - \mathscr{K}\mathbf{q} - \mathscr{L}\dot{\mathbf{q}} - \dot{\theta}^2\Phi^t M\mathscr{L}_1 \sin\theta_2 + (\theta_1 + \theta_2)\mathbf{q}, \tag{39}$$

$$D = (I_{11} - I_{1q}I_{q1})(I_{22} - I_{2q}I_{q2}) - (I_{12} - I_{2q}I_{q1})(I_{12} - I_{1q}I_{q2}), \tag{40}$$

$$L_1 = \mathbf{N_P}\mathscr{L}_1 = \mathbf{N_P}[L_1, \ldots, L_1]^{\mathrm{t}}, \tag{41}$$

$$\mathscr{K} = \mathbf{\Phi}^{\mathrm{T}}\mathbf{K}\mathbf{\Phi} = \mathrm{diag}(\omega_i^2), \tag{42}$$

$$\mathscr{C} = \mathrm{diag}\,(2\xi_i\omega_i) \tag{43}$$

and the equation of the piezoelectric/mechanical coupling is given by

$$\mathscr{A}^{\mathrm{t}}\mathbf{q} + \mathbf{\Lambda}\mathbf{v} = -\mathbf{q}_e \tag{44}$$

with

$$\mathscr{A} = \mathbf{\Phi}^{\mathrm{t}}\mathbf{\Pi}. \tag{45}$$

To separate the sensor and actuator ceramics parameters in (29)–(31), the indices c and a are used in the corresponding symbols, hence (44) can be factorized into

$$\mathscr{A}_a^{\mathrm{t}}\mathbf{q} + \mathbf{\Lambda}_a\mathbf{v}_a = -\mathbf{q}_{ea} \tag{46}$$

$$\mathscr{A}_c^{\mathrm{t}}\mathbf{q} + \mathbf{\Lambda}_c\mathbf{v}_c = -\mathbf{q}_{ec} \tag{47}$$

with:

$$\mathbf{q}_e = \begin{bmatrix} \mathbf{q}_{ea} \\ \mathbf{q}_{ec} \end{bmatrix}, \quad \mathscr{A} = [\mathscr{A}_a\ \mathscr{A}_c], \quad \mathbf{v} = \begin{bmatrix} \mathbf{v}_a \\ \mathbf{v}_c \end{bmatrix} \quad \text{and} \quad \mathbf{\Lambda} = \begin{bmatrix} \mathbf{\Lambda}_a & 0 \\ 0 & \mathbf{\Lambda}_c \end{bmatrix}. \tag{48}$$

Conditioning carried out by the charge amplifiers of the signals of the sensors ($\mathbf{q}_{ec} = 0$), (29–31) become

$$\mathbf{v}_c = -\mathbf{\Lambda}_c^{-1}\mathscr{A}_c^{\mathrm{t}}\mathbf{q} \tag{49}$$

which, introduced into (39) implies

$$\mathbf{C}_q = \mathbf{A}_a\mathbf{v}_a - \mathscr{K}_c\mathbf{q} - \mathscr{L}\dot{\mathbf{q}} - \dot{\theta}_1^2\Phi^t\mathbf{M}\mathscr{L}_1 \sin\dot{\theta}_2 + \dot{\theta}_1 + \dot{\theta}_2)2\mathbf{q} \tag{50}$$

with the matrix of modal stiffness $\mathscr{K}_c$ including the feedback effect of the ceramics sensors

$$\mathscr{K}_c = \mathscr{K} + \mathscr{A}_c\mathbf{\Lambda}_c^{-1}\mathscr{A}_c^t. \tag{51}$$

This model was programmed in MATLAB-SIMULINK. Before simulations, linear representations are carried out with the included algorithm, and simulations of non-controlled and controlled dynamic behavior are carried out using the algorithm ode45 which is based on an explicit Runge–Kutta (4,5) formula, the Dormand–Prince pair.

4. Control of a rigid bi-articulated structure

In the model presented above, the flexible beam 2 is replaced here by a rigid bar. It is set in motion and controlled by two motor reducers delivering the respective torques C_{m_1} and C_{m_2} while the rotation of each bar $\boldsymbol{\theta}_1$ and $\boldsymbol{\theta}_2$ is measured directly. The motion equations of the rigid

bi-articulated structure are obtained from (29) and (30) by identifying $\mathbf{q}$ and $\dot{\mathbf{q}}$ by zero, thus

$$\theta_1 = [I_2(C_{m_1} + N_1) - I_{12}(C_{m_2} + N_2)]/(I_{11}I_2 - I_{12}^2), \tag{52}$$

$$\dot{\theta}_2 = [I_{11}(C_{m_2} + N_2) - I_{12}(C_{m_1} + N_1)]/(I_{11}I_2 - I_{12}^2) \tag{53}$$

with:

$$I_{11} = I_1 + I_2 + m_1L_1^2 + m_2L_1L_2 \cos \boldsymbol{\theta}_2; \tag{54}$$

$$I_{12} = I_2 + m_2L_1L_2(\cos \boldsymbol{\theta}_2)/2, \tag{55}$$

$$N_1 = m_2L_1L_2 \sin \theta_2(\dot{\theta}_1 + \dot{\theta}_2)\dot{\theta}_2, \tag{56}$$

$$N_2 = -m_2L_1L_2\dot{\theta}_1^2(\sin \dot{\theta}_2)/2. \tag{57}$$

Eq. (52) and (53) are rewritten in the following state form:

$$\dot{\mathbf{x}} = \mathbf{Ax} + \mathbf{Bu} + \mathbf{p} = \frac{\mathrm{d}}{\mathrm{d}t}\begin{Bmatrix} \boldsymbol{\theta} \\ \boldsymbol{\theta}_2 \\ \dot{\boldsymbol{\theta}}_1 \\ \dot{\boldsymbol{\theta}}_2 \end{Bmatrix} = \begin{bmatrix} 0 & 0 & 1 & 0 \\ 0 & 0 & 0 & 1 \\ 0 & 0 & 0 & 0 \\ 0 & 0 & 0 & 0 \end{bmatrix}\begin{Bmatrix} \dot{\boldsymbol{\theta}}_1 \\ \boldsymbol{\theta}_2 \\ \dot{\boldsymbol{\theta}}_1 \\ \dot{\boldsymbol{\theta}}_2 \end{Bmatrix} + \begin{bmatrix} 0 & 0 \\ 0 & 0 \\ B_{11} & B_{12} \\ B_{21} & B_{22} \end{bmatrix}\begin{Bmatrix} C_{m_1} \\ C_{m_2} \end{Bmatrix} + \begin{Bmatrix} 0 \\ 0 \\ Nl_1 \\ Nl_2 \end{Bmatrix} \tag{58}$$

with

$$B_{11} = \frac{I_{22}}{I_{11}I_{22} - I_{12}^2};\ \ B_{12} = B_{21} = \frac{-I_{12}}{I_{11}I_{22} - I_{12}^2};\ \ B_{22} = \frac{I_{11}}{I_{11}I_{22} - I_{12}^2} \tag{59}$$

$$Nl_1 = \frac{I_{22}N_1 - I_{12}N_2}{I_{11}I_{22} - I_{12}^2};\ \ Nl_2 = \frac{I_{11}N_2 - I_{12}N_1}{I_{11}I_{22} - I_{12}^2}. \tag{60}$$

For the characteristics of the structure given in Table 1, terms Nl_i of vector $\mathbf{p}$, which models centrifugal type effects, are slightly nonlinear, whereas terms $\mathbf{B}_{ij}$ of the matrix $\mathbf{B}$, whose progression is shown in Fig. 4, are strongly nonlinear.

The adaptive controller is established from (5) by using the nine linearization points (4). tatic precision is ensured by an integrator on each variation of rigid body displacements θ_1 and θ_2, with the rotation set points θ_{10} and θ_{20} to be reached

$$\mathbf{y}_c = \begin{Bmatrix} \dot{\theta}_1 \\ \dot{\theta}_2 \end{Bmatrix};\ \ \mathbf{z} = \begin{Bmatrix} \dot{\theta}_{10} \\ \dot{\theta}_{20} \end{Bmatrix}. \tag{61}$$

Table 1
Bi-articulated rigid structure characteristics

Characteristics	Rod 1	Rod 2
Length (m)	$L_1 = 0.5$	$L_2 = 0.5$
Mass (kg)	$m_1 = 0.09$	$m_2 = 0.09$
Inertia (kg m^2)	$I_1 = 19 \times 10^{-4}$	$I_2 = 19 \times 10^{-4}$

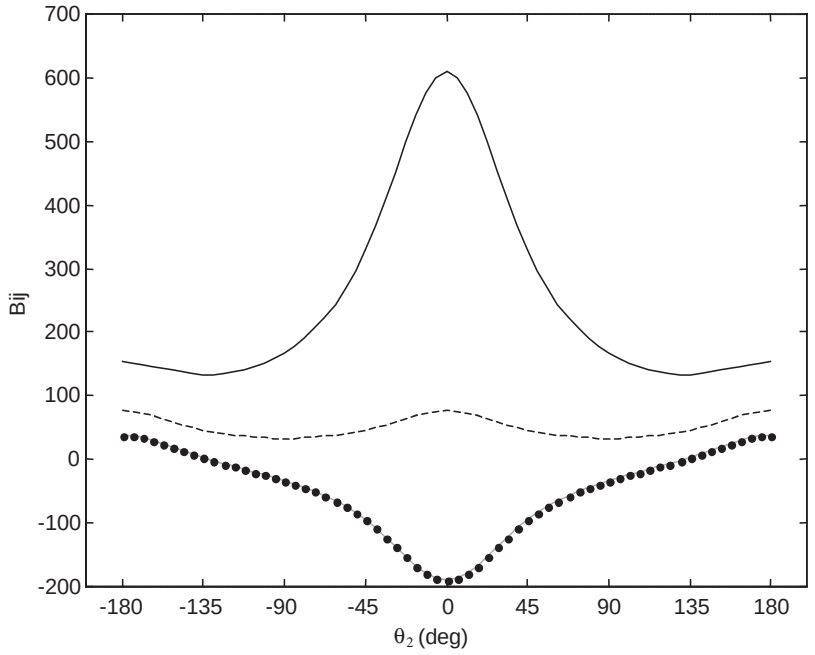

Fig. 4. Progression of B matrix coefficients (------: B_{11}, ——: B_{12}, ●●●●●: B_{21}, ——: B_{22}).

The augmented state $\mathbf{x}_a$ is thus described by

$$\mathbf{x}_a = \left[\theta_1, \theta_2, \dot{\theta}_1, \dot{\theta}_2, \int (\theta_1 - \theta_{10})\,\mathrm{d}t, \int (\theta_2 - \theta_{20})\,\mathrm{d}t\right]^t. \tag{62}$$

The selected weight functions f_i are linear. They give the fields of action of the linear controllers presented in Fig. 3. For each operating point i, the gains matrices $\mathbf{G}_i$ are calculated by using matrices $\mathbf{A}_i$ and $\mathbf{B}_i$ of the corresponding linearized models (1), and the diagonal weighting matrices $\mathbf{Q}_i$ and $\mathbf{R}_i$ of the performance index J_i (9).

The first adjustment of weightings is carried out independently for each controller in order to optimize the elimination of the disturbances for any geometrical configuration. The robustness of both stability and performance can thus be modulated according to the geometrical configuration. Here, the objective is to obtain a nearly constant damping and close to critical damping for any configuration of the structure, as well as maximum rigidity and perfect static precision. First of all, the adjustment principle is to adjust the first linear controller on the basis of the temporal simulations around position $\theta_2 = 0$, by choosing each of the 6 weightings $\mathbf{Q}_0$ and the 2 weightings $\mathbf{R}_0$. The adjustment of the weightings for this position is then optimized by using a temporal template. Then, the adjustment of weightings $\mathbf{Q}_i$ and $\mathbf{R}_i$, used in the performance index (9) of the other controllers is optimized frequentially in order to obtain the same damping for the poles in a closed loop. Since the progression of the dynamic behavior of the structure must be symmetrical in relation to position $\theta_2 = 0$, the symmetry of the weightings therefore limits the adjustments to operating points $i = \pi/8,\ \pi/4,\ 3\pi/8,\ \pi/2$. The $8 \times 5 = 40$ weightings chosen after temporal

Table 2
Weight for each linear controller for the "same damping" adjustment—rigid bi-articulated structure

$i=\theta_2$	Weight							
(operating point)	q_{11}	q_{22}	q_{33}	q_{44}	q_{55}	q_{66}	r_{11}	r_{22}
0	$6.65e^4$	$6.64e^3$	$1.24e^2$	$5.13e^0$	$2.99e^7$	$3.19e^6$	9.98	3.74
$\pi/8$ and $-\pi/8$	$2.15e^5$	$3.46e^4$	$2.34e^2$	$2.58e^1$	$8.80e^7$	$1.66e^7$	44.2	13.1
$\pi/4$ and $-\pi/4$	$2.50e^4$	$4.27e^3$	$2.14e^1$	$2.86e^0$	$1.04e^7$	$2.04e^6$	6.56	0.518
$3\pi/8$ and $-3\pi/8$	$1.26e^4$	$2.71e^3$	$3.87e^0$	$1.18e^0$	$5.29e^6$	$1.28e^6$	5.74	0.281
$\pi/2$ and $-\pi/2$	$2.20e^5$	$5.05e^4$	$1.60e^2$	$2.75e^1$	$8.43e^7$	$2.42e^7$	178	9.75

optimization and the 4 frequential optimizations reduced to the calculation of the poles alone, are given in Table 2 based on a disturbance in steps of 2 and 1 Nm, respectively, on torques C_{m_1} and C_{m_2}.

Fig. 5 presents the position of the poles in the complex plane as the geometrical configuration of the structure moves. The results show the sliding of the poles in closed loop when rotation θ_2 changes. In the case of a fixed linear controller established for $\theta_2 = 0$, the loss of damping is significant and the position of the poles moves considerably, revealing significant change of the dynamic behavior of the controlled structure, to the detriment of the stability margin. In the case of the adaptive controller calculated for the operating points and $i=0$, $\pi/4$, and $\pi/2$ with linear weighting functions f_i, the poles are maintained close to constant damping, with a controlled progression of speed, revealing a slight change of dynamics in spite of the geometrical modification of the structure: the dynamics obtained is therefore robust in terms of stability and performance.

Fig. 6 presents the temporal responses of the linear $\theta_2 = 0$ and adaptive controllers during disturbance steps of 2 and 1 Nm, respectively on torques C_{m_1} and C_{m_2}. The effectiveness of the controllers for a zero fixed control is tested by simulating the responses around position $\theta_1 = 0$ of the first bar and for the positions of the second bar. To achieve this, the position order $\mathbf{z}$ is equal to the initial position $(0, \theta_{20})$. The linear controller shows a significant loss of performance as the structure moves away from the linearization point ($\theta_2 = 0$). On the other hand, the adaptive controller maintains the same equilibrium establishment times and the same damping for the various disturbance positions θ_{20} .

The second adjustment of weightings aims at optimizing the time of equilibrium establishment during the tracking of set points ($\theta_1 = 180^\circ, \theta_1 = 90^\circ$) while limiting the global command of the actuators to 5 Nm. In this case, the tracking is established by sweeping the various operating points, and by making all the linear controllers participate during the motion of the structure. The adjustment principle is based on the simultaneous optimization of the weightings of all the linear controllers by using a temporal gauge. Taking into account the symmetries, the simultaneous optimization of the significant number of weightings was reduced by considering only three different linear controllers, corresponding to the operating points of: $\theta_2=0$, $\pi/4$, $\pi/2$. Optimization concerns 24 parameters. The weightings chosen after temporal optimization are given in Table 3.

Fig. 7 presents the temporal curves of the responses and the commands for this second adjustment. The time of equilibrium establishment while tracking of set points ($\theta_1 = 180^\circ, \theta_1 = 90^\circ$)

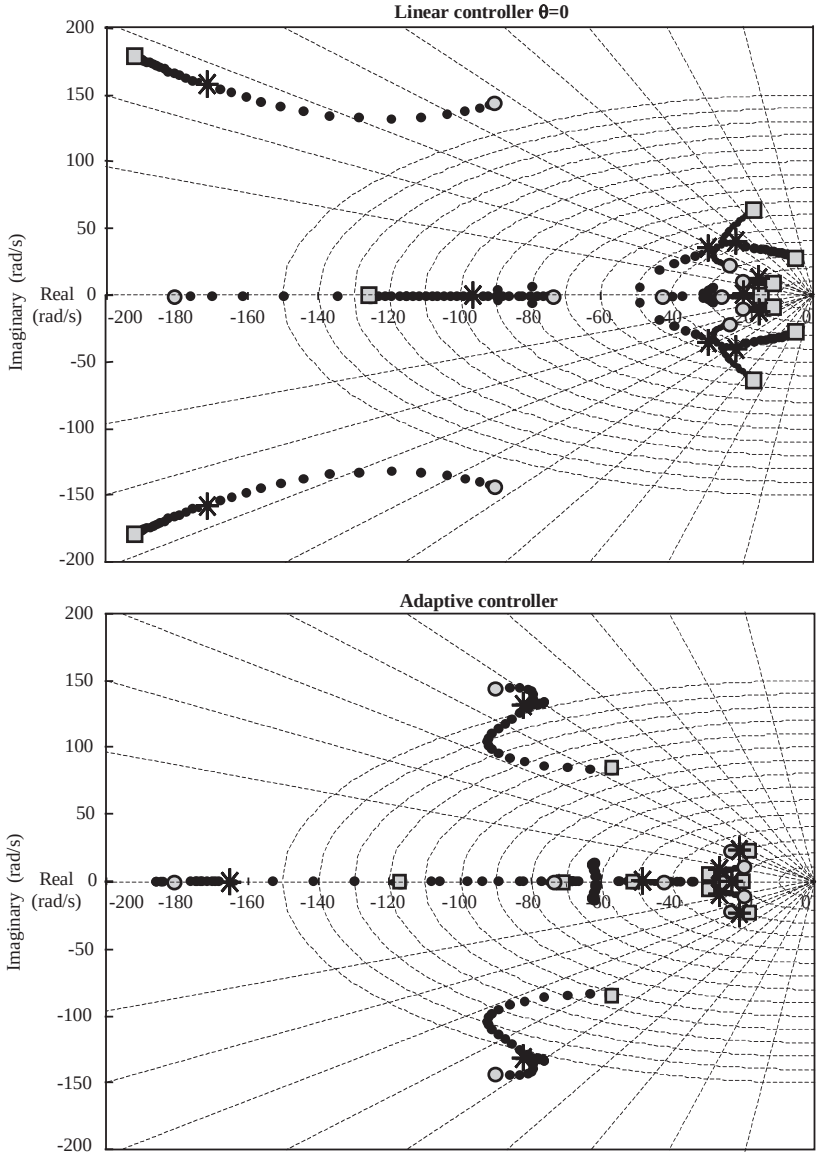

Fig. 5. Sliding of the close feedback poles as a function θ_2 (□: 0, ✳: p/4, ○: p/2, ●: Others).

to the adaptive controller is much faster than that of all the linear controllers ($\theta_2 = 0$)and $\pi/2$ presented here). Indeed, the adaptive controller allows optimizing the use of the engines by using powers higher than those of the linear controllers, in particular, at the beginning of the movement (see the torques Fig. 7).

In the case of two rigid bars, the adaptive controller proposed is more efficient than the linear controllers, for control and during the tracking. Moreover, it guarantees stability and makes it possible to obtain flexible dynamics according to the motion of the bi-articulated structure.

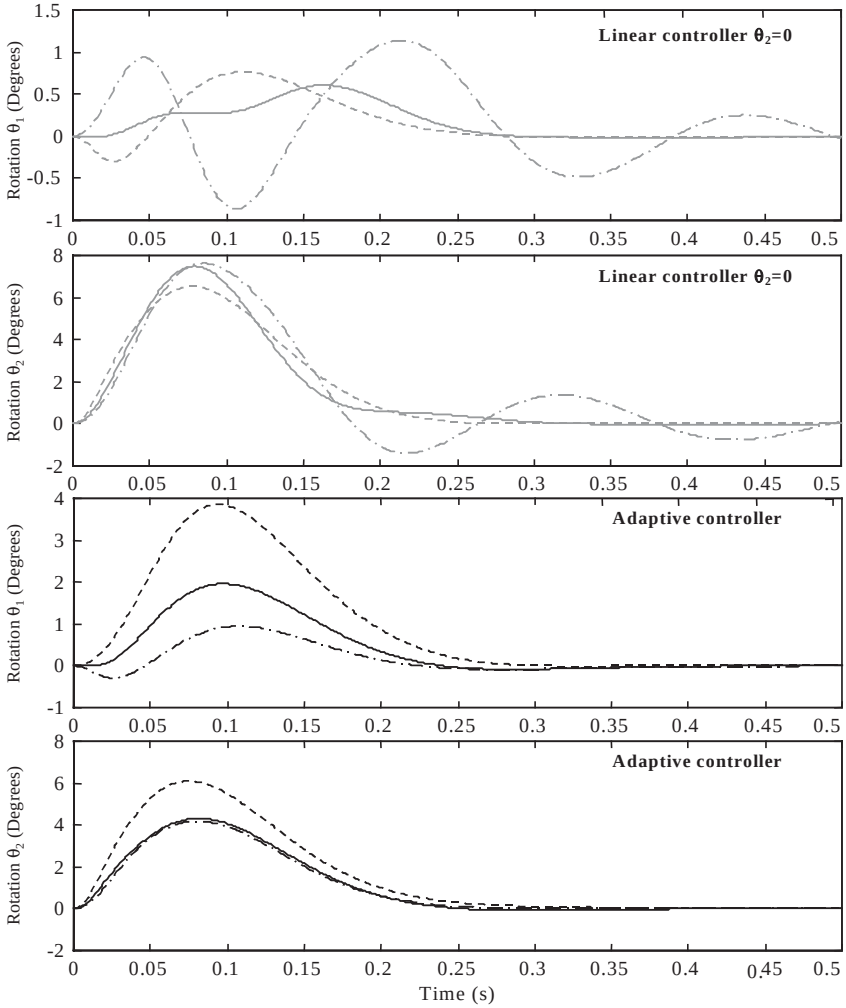

Fig. 6. Responses of the rigid bi-articulated structure—first adjustment (step disturbance C_{m1}: 2 Nm; C_{m2}: 1 Nm) (----: $\theta_{20}=0$, ——: $\theta_{20}=\pi/4$, —·— : · $\theta_{20}=\pi/4$).

Table 3
Weight for each linear controller for the second adjustment (set points tracking $\theta_1 = 180^\circ, \theta_1 = 90^\circ$)—rigid bi-articulated structure

$i=\theta_2$	Weight							
(operating point)	q_{11}	q_{22}	q_{33}	q_{44}	q_{55}	q_{66}	r_{11}	r_{22}
0	$3.24e^{1}$	$1.97e^{1}$	$9.10e^{-5}$	$5.37e^{-3}$	$2.40e^{1}$	$3.80e^{2}$	$2.18e^{-3}$	$9.60e^{-3}$
$\pi/4$ and $-\pi/4$	$2.16e^{0}$	$1.16e^{0}$	$7.97e^{-5}$	$2.90e^{-2}$	$4.68e^{2}$	$2.04e^{3}$	$1.78e^{-1}$	$6.06e^{-3}$
$\pi/2$ and $-\pi/2$	$5.18e^{0}$	$4.26e^{1}$	$7.51e^{-5}$	$2.34e^{-3}$	$4.21e^{2}$	$5.45e^{3}$	$7.85e^{-2}$	$6.06e^{-3}$

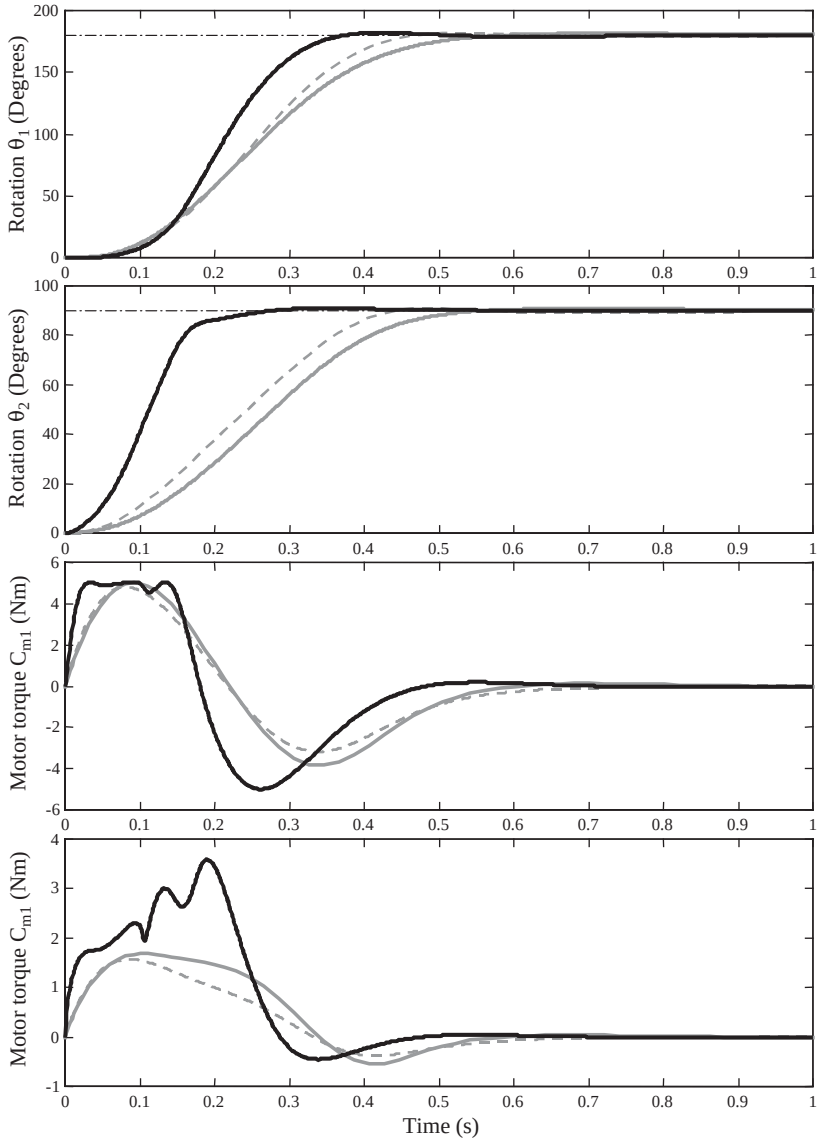

Fig. 7. Responses and commands—second adjustment (set points tracking ($\theta_1 = 180°$, $\theta_1 = 90°$) (- - -: Linear ($\theta_2 = 0$), ——: Linear ($\theta_2 = \pi/2$), ——: Adaptive, – · – · –: Step order).

5. Control of flexible bi-articulated structures

The control principle presented above (Section 2) can be applied to mono or multi-articulated flexible structures by adapting the modeling detailed in Section 3. In this case, taking into account the limited band-width of the motor reducers, it is necessary to finalize their action by using piezoelectric actuators (here piezoelectric patches stuck on the structure), that control the flexible modes outside the band-width of the engines. The design proposed for the instrumented flexible

structures includes four piezoelectric ceramics. Two ceramics constitute a bimorph actuator while the two others are used as strain sensors. The characteristics of these components are given Table 4. The objective selected for control is to perform the rotation command as quickly as possible, without static stress generated by the piezoelectric actuators, while damping the vibrations of the first flexible modes of the flexible beam to the maximum, and without destabilizing the other modes.

The model of structure (29–31) developed under Ansys® comprises the FE model of the structure provided with ceramic sensors and actuators (Fig. 8). The types of FE which discretize it were selected in order to guarantee their connection. The discretized beam is composed of 43 volume elements (SOLID 45) with eight nodes with three degrees of freedom (dof) per node. Piezoelectric actuators and sensors are respectively meshed by 4 and 3 volume elements (SOLID 5) with eight nodes with three translation (dof) and one electric potential (dof) per node. The electric potentials of all the nodes of the beam/ceramic sensor are constrained to zero, and those of the nodes of each external face set at the same potential as the uniform potential of the corresponding silver electrode. The potential of the ceramic actuators is kept at 0 V and those of the ceramic sensors is left free in order to allow piezoelectric feedback. Then the FE 3D model was condensed into 42 master nodes.

Table 4
Characteristics of the components

Parameter	Value	Unit
Rod 1		
Length (L_1)	500	mm
Mass (m_1)	0.9	kg
Inertia (I_1)	7.5×10^{-2}	$\mathrm{kg\,m^2}$
Beam 2		
Length (L_2)	715	mm
Width	30	mm
Thickness	2	mm
Young's modulus	69 000	MPa
Density	2770	$\mathrm{kg\,m^{-3}}$
Mass (m_2)	160	g
Inertia (I_2)	4.2×10^{-2}	$\mathrm{kg\,m^2}$
Piezoelectric ceramics		
Actuator length	70	mm
Sensor length	40	mm
Width	25	mm
Thickness	0.5	mm
Young's modulus	114 000	Mpa
Density	7460	$\mathrm{kg\,m^{-3}}$
Piezoelectric constant(d_{31})	-127×10^{-12}	$\mathrm{mV^{-1}}$
Motor/reducers		
Inertia(I_0)	344×10^{-5}	$\mathrm{kg\,m^2}$

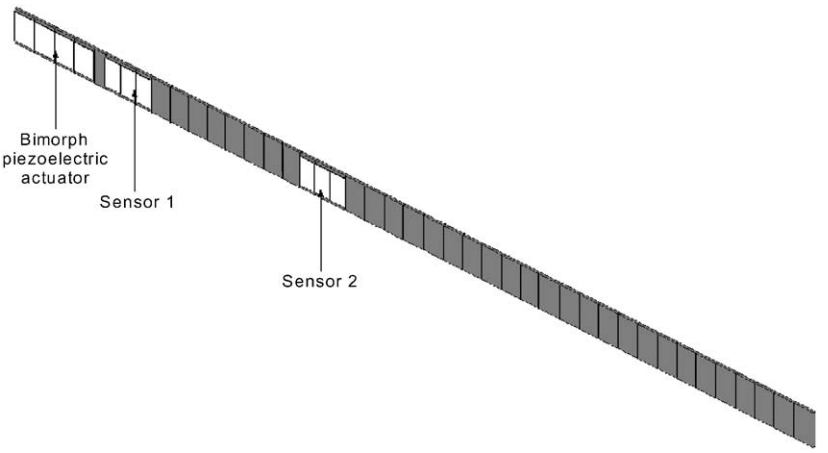

Fig. 8. Finite element model of the flexible beam

At first, a modal study was carried out to obtain the $\mathscr{M}$ modal mass matrix, $\mathscr{K}_c$ modal stiffness, mode shape Φ, and modal forms of the electric potentials of the sensors $\mathscr{A}_c$. A static study was then carried out to obtain the modal activation vector $\mathscr{A}_a$ of the bimorph actuator. Thus the potentials of + 1 and –1 V, respectively, were applied to each ceramic composing the actuator. The equilibrium of the structure was then obtained from

$$\mathscr{K}_c q_a = \mathscr{A}_a \tag{63a}$$

$$\boldsymbol{\delta}_a = \boldsymbol{\Phi}\mathbf{q}_a \tag{63b}$$

with $\mathbf{q}_a$ being the modal participations of static displacement $\boldsymbol{\delta}_a$ of the master dof calculated by projection on the modal basis

$$q_a = (\boldsymbol{\Phi}^t\boldsymbol{\Phi})^{-1}\boldsymbol{\Phi}^t\delta_a. \tag{64}$$

The activation vector was then obtained by

$$\mathscr{A}_a = \mathscr{K}_c(\boldsymbol{\Phi}^t\boldsymbol{\Phi})^{-1}\boldsymbol{\Phi}^t\delta_a. \tag{65}$$

The model of the flexible beam instrumented, clamped–free, obtained for null rotations θ_1 and θ_2, was accurately fitted by optimization based on experiments implementing the piezoelectric actuators and sensors and with a displacement sensor at the end of the beam [27]. The mode shapes and the frequencies obtained after optimized fitting are given Fig. 9.

5.1. Mono-articulated flexible beam

The model of the clamped–free instrumented flexible beam was used to carry out the control of the rigid body mode and the first two flexible modes of a mono-articulated flexible structure clamped on the rotor of a motor reducer. The control carried out by an engine and a bimorph piezoelectric actuator, a potentiometer of precision and two piezoelectric ceramics sensors, is presented in [27].

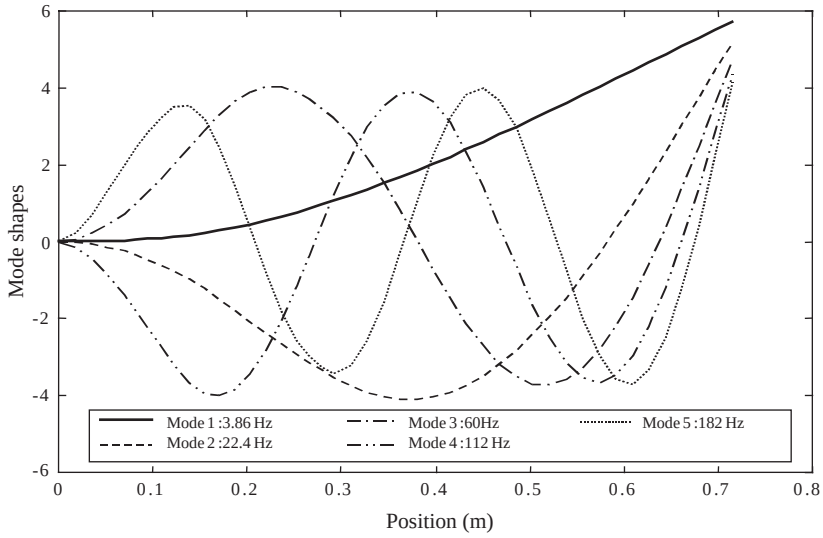

Fig. 9. Mode shapes and resonance frequencies—clamped–free beam.

The beam is mono-articulated, so the non linearities induced by the variation of inertia around $(A, \mathbf{z}_0)$ during the rotation of the second beam do not exist. The controller was thus limited to only one linear controller. The control objectives here are to carry out a rotation set point tracking precisely and as quickly as possible, by damping out the vibrations to the maximum and by eliminating any permanent curvature.

To calculate the controller, the model was linearized and put in state form. In order to obtain good precision in the performance of the rotation set point tracking, and a null static curvature of the beam, the state $(\theta_1, \mathbf{q}, \dot{\theta}_1, \dot{\mathbf{q}})$ was augmented by the integral of the rigid body rotation variation $\int(\theta_1 - z)\,\mathrm{d}t$ and by the integral $\int(\theta_1 - z)\,\mathrm{d}t$ of the piezoelectric actuator control v_a. After temporal optimization starting from a template (see [27]), the weightings selected for the controller Q and R, and for the observer Q_{obs} and R_{obs} are:

$$
\begin{aligned}
Q &= \mathrm{diag}\,(\,2.47^3 \quad 1.0^8 \quad 1.0^7 \quad 0.752 \quad 2.69^3 \quad 1.53^4 \quad 2.61^4 \quad 1.0^2\,),\\
R &= \mathrm{diag}\,(\,25 \quad 50\,),\\
Q_{\mathrm{obs}} &= \mathrm{diag}\,(\,1^6 \quad 1 \quad 0.1 \quad 1^6 \quad 1^3 \quad 1^3\,),\\
R_{\mathrm{obs}} &= \mathrm{diag}\,(\,0.5 \quad 0.5 \quad 0.5 \quad 0.5\,).
\end{aligned}
\tag{66}
$$

The bench used for the control of the dynamic behavior of the mono-articulated flexible structure is presented in Fig. 10. The results of the experiment corresponding to the adjustment (66) and for the 120° rotation set point tracking can be compared in Fig. 11 with those given by corresponding simulations.

The comparison of the results shows that the experiment validates the simulations carried out based on a model accurately fitted by three successive optimizations. The control obtained is

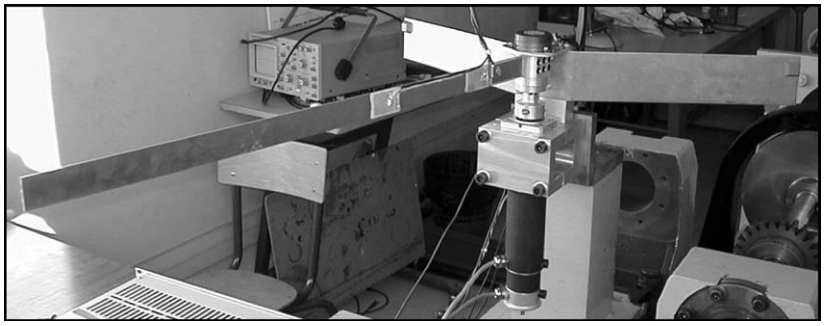

Fig. 10. Experimental set-up of the instrumented mono-articulated flexible structure.

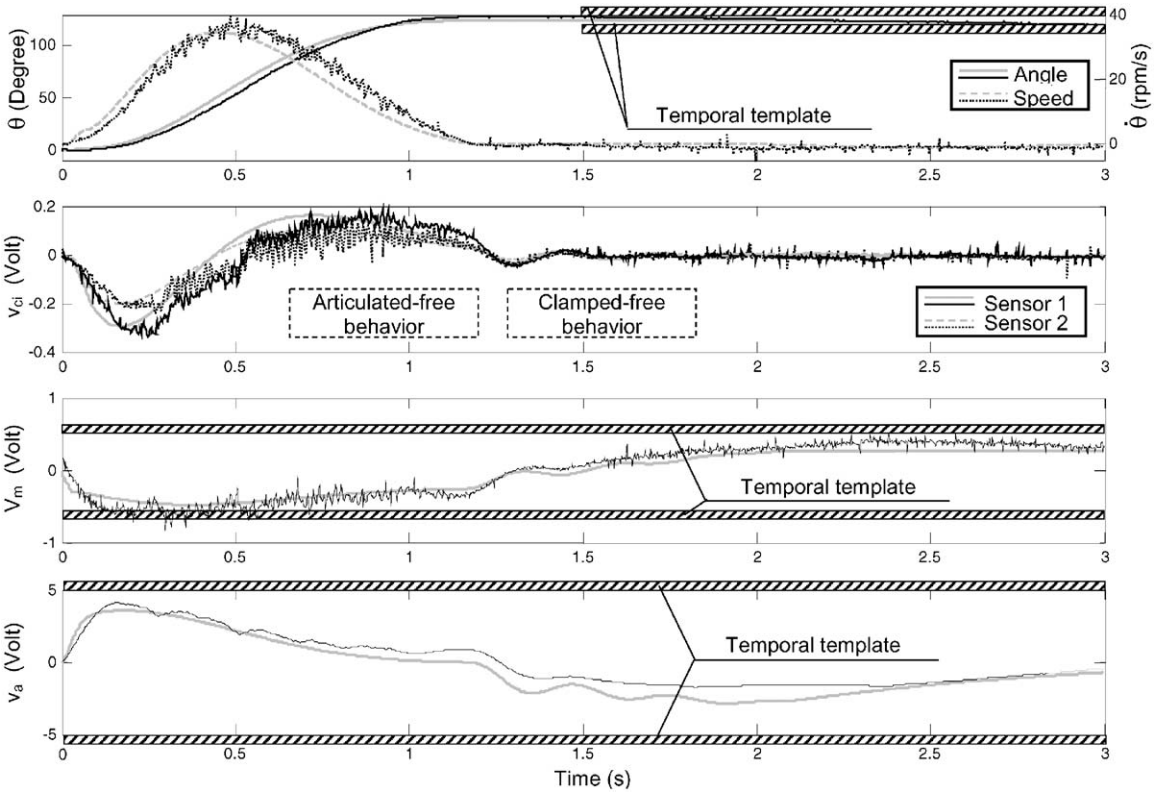

Fig. 11. Simulated and measured responses and commands of the controlled mono-articulated flexible structure—120° step set point tracking.

efficient. The tracking is performed quickly and precisely with significant damping of vibrations. Indeed, modal damping slips from 0, 0.48, 0.42 to 13, 4.5, 1.4, respectively, at frequencies 0, 3.93 and 22.4 Hz.

Since friction in the motor reducer is opposed to the rotation of the structure, the dynamic behavior slips from "supported–free" to "clamped–free" to 1.05 s. In this case, the flexible modes

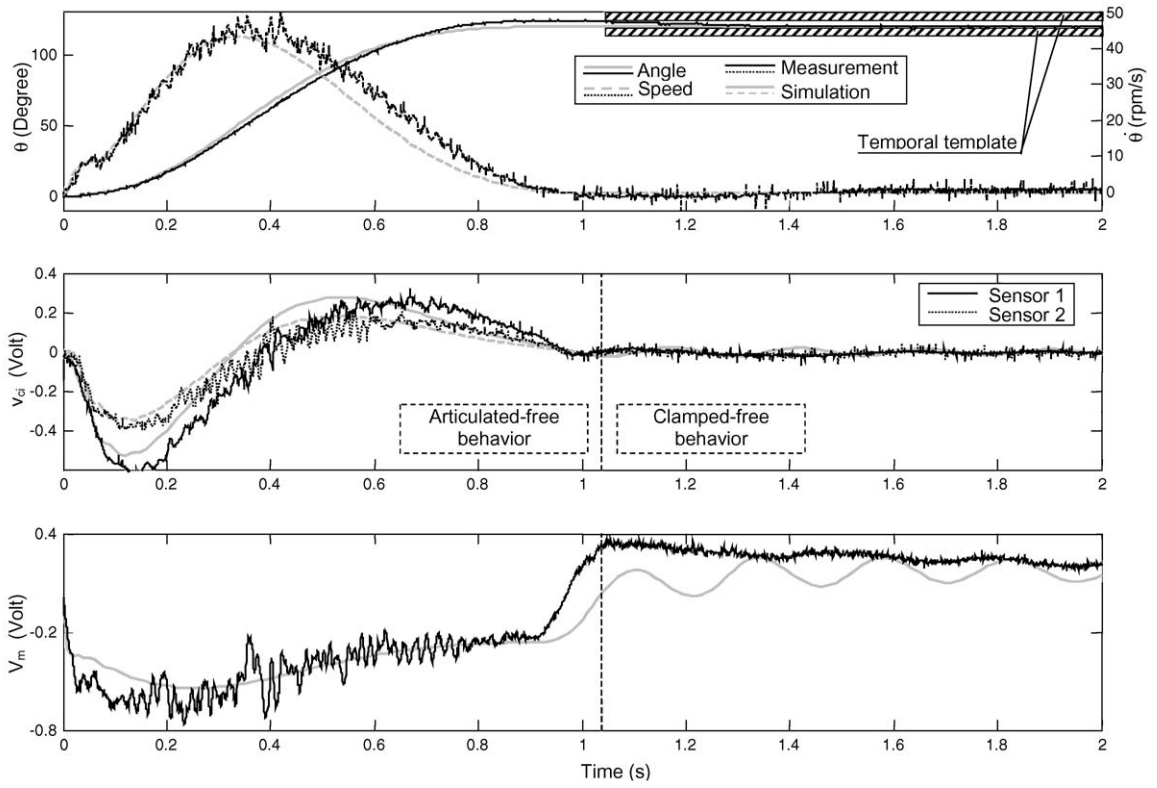

Fig. 12. Simulated and measured responses and commands of the controlled mono-articulated flexible structure—120° step set point tracking—operated without a piezoelectric actuator.

are wholly controlled by the piezoelectric actuators. Their effectiveness is shown in Fig. 12, where the same rotation set point tracking is carried out, but without any action by the piezoelectric actuator.

For the mono-articulated structures, whose vibrations are coupled with rigid body displacements and whose technological choices prove adapted, the results therefore show that global linear control is adapted and effective when modeling is done accurately (optimized fitting).

5.2. *Bi-articulated flexible structure*

In this part of the study, the structure presented in Fig. 1, which has strongly nonlinear behavior caused by the modification of its moment of inertia around $(A, \vec{z}_0)$ during the rigid body rotation of beam 2, the model proposed in Section 2, and the adaptive control method presented Section 1 are used . The selected control objectives are to perform the rotation set point tracking as quickly as possible, while controlling the vibrations of the two rigid body modes and the first five flexible modes of beam 2, in particular at the end of the structure, by eliminating permanent strain.

The adaptive controller is based on (5) by taking the nine points of linearization (4) into account. To calculate the controller, the model was linearized on each operating point and put in state form (1).

Static precision is ensured by an integrator on each variation between rigid body displacements θ_1 and θ_2 and the rotation set point tracking θ_{10} and θ_{20} to be performed, and by the integral $\int v_a \, dt$ of the control v_a of the piezoelectric actuator, to ensure a null curvature. Thus the state vector used by the controller is

$$\mathbf{x}_a = \left[\theta_1 \; \theta_2 \; q_1 \; q_2 \; q_3 \; q_4 \; q_5 \; \theta_2 \; \dot{\theta}_2 \; \dot{q}_1 \; \dot{q}_2 \; \dot{q}_3 \; \dot{q}_4 \; \dot{q}_5 \; \int (\theta_1 - \theta_{10}) \, dt \; \int (\theta_2 - \theta_{20}) \, dt \; \int v_a \, dt\right]^t. \quad (67)$$

As previously, the selected weight functions f_i are linear. They give the action field of the linear controllers presented Fig. 3. For each operating point i, the gains matrices G_i are calculated starting from matrices $\mathbf{A_i}$ and $\mathbf{B}_i$ of the corresponding linearized models (1), and the diagonal weighting matrices $\mathbf{Q}_i$ and $\mathbf{R}_i$ of the performance index J_i (9).

In order to reduce the number of weightings to be regulated, weightings a_3 on the flexible modes are selected as identical on the modal participations in displacement. In addition, weightings a_6 of the modal participations of the speed selected are coupled by the intermediary of $\boldsymbol{\omega}$ containing the pulsations of each mode, in order to ensure the identical damping of each mode in feedback mode

$$\mathbf{Q}_i = \mathrm{diag}[a_1 \quad a_2 \quad \overbrace{[a_3 \quad \ldots \quad a_3]}^{5\text{times}} \quad a_4 \quad a_5 \quad a_6[\boldsymbol{\omega}]^t \quad a_7 \quad a_8 \quad a_9]. \quad (68)$$

Consequently, there are 12 weightings per linear controller and a total of 60 to be regulated.

The first adjustment of weightings is carried out independently for each controller in order to optimize the elimination of the disturbances for all the geometrical configurations met. The weightings of the linear controller establsihed for position $\theta_2 = 0$ are adjusted by temporal optimization starting from a template

$$\mathbf{Q}_i = \mathrm{diag}[7 \times 10^5 \quad 7 \times 10^4 \quad \overbrace{[10^9 \quad \ldots \quad 10^9]}^{5\text{times}} \quad 10^3 \quad 5 \quad 60 \times [\boldsymbol{\omega}]^t \quad 3 \times 10^8 \quad 3 \times 10^7 \quad 10]. \quad (69)$$

These weightings are re-used for the calculation of the other controllers, giving different gains $\mathbf{G}_i$ (10) by using the Riccati equation (11), solved with state matrices $\mathbf{A}_i$ and $\mathbf{B}_i$ corresponding to each operating point crossed.

Fig. 13 shows the sliding of the position of the poles in the complex plane when θ_2 progresses in the case of the linear controller established for $\theta_2 = 0$, and the adaptive controller. In the case of the linear controller established for $\theta_2 = 0$, the loss of damping and the progression of rapidity are significant. Some poles move towards a positive real part corresponding to instability. In the case of the adaptive controller proposed, the poles of the structure are maintained in the same place, confirming the constant damping and rapidity of each one. Only the poles of the integrators move in order to obtain an identical time of establishment for each position. All the poles are maintained in the complex half plane with a negative real part that characterizes stable control.

Fig. 14 presents the responses θ_1, θ_2, and displacement $\boldsymbol{\delta}_{\mathrm{ext}}$ at the end of beam 2 of the structure controlled by the linear controller established for $\theta_2 = 0$ and by the adaptive controller proposed.

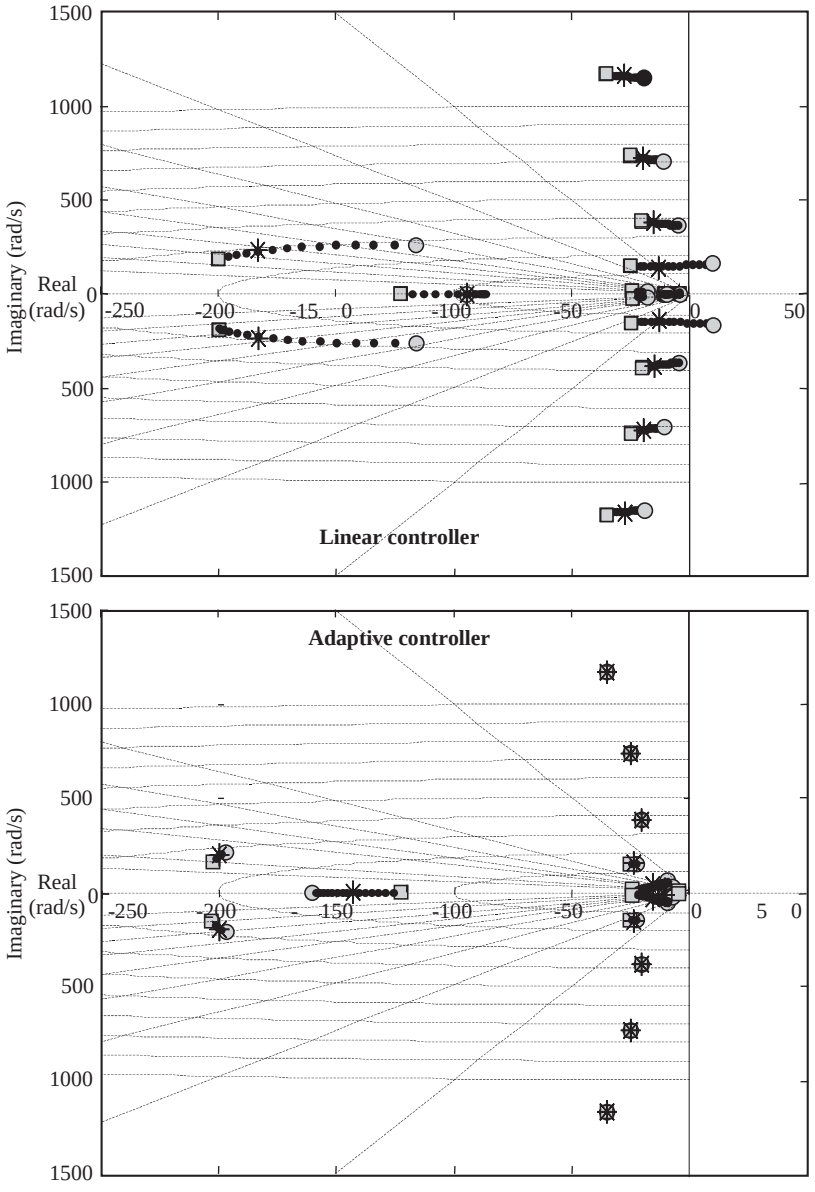

Fig. 13. Sliding of the close feedback poles of bi-articulated flexible structure as a function θ_2 (□: 0, ✳: p/4, ○: p/2, ●: Others).

The disturbance generated at θ_{20} on the torques of the motor reducers is a step: $C_{m_1} = 2$ Nm and $C_{m_2} = 1$ Nm. Simulations show that the damping of the dynamic behavior of the structure controlled by the linear controller established for $\theta_2 = 0$ decreases as the distance of the disturbance generated from $\theta_2 = 0$ increases. The motion continues until instability for $\theta_2 = 70^\circ$ and beyond. On the other hand, the adaptive controller maintains the same disturbance rejection times, with the same damping, and is not unstable whatever the case. The dynamics of the

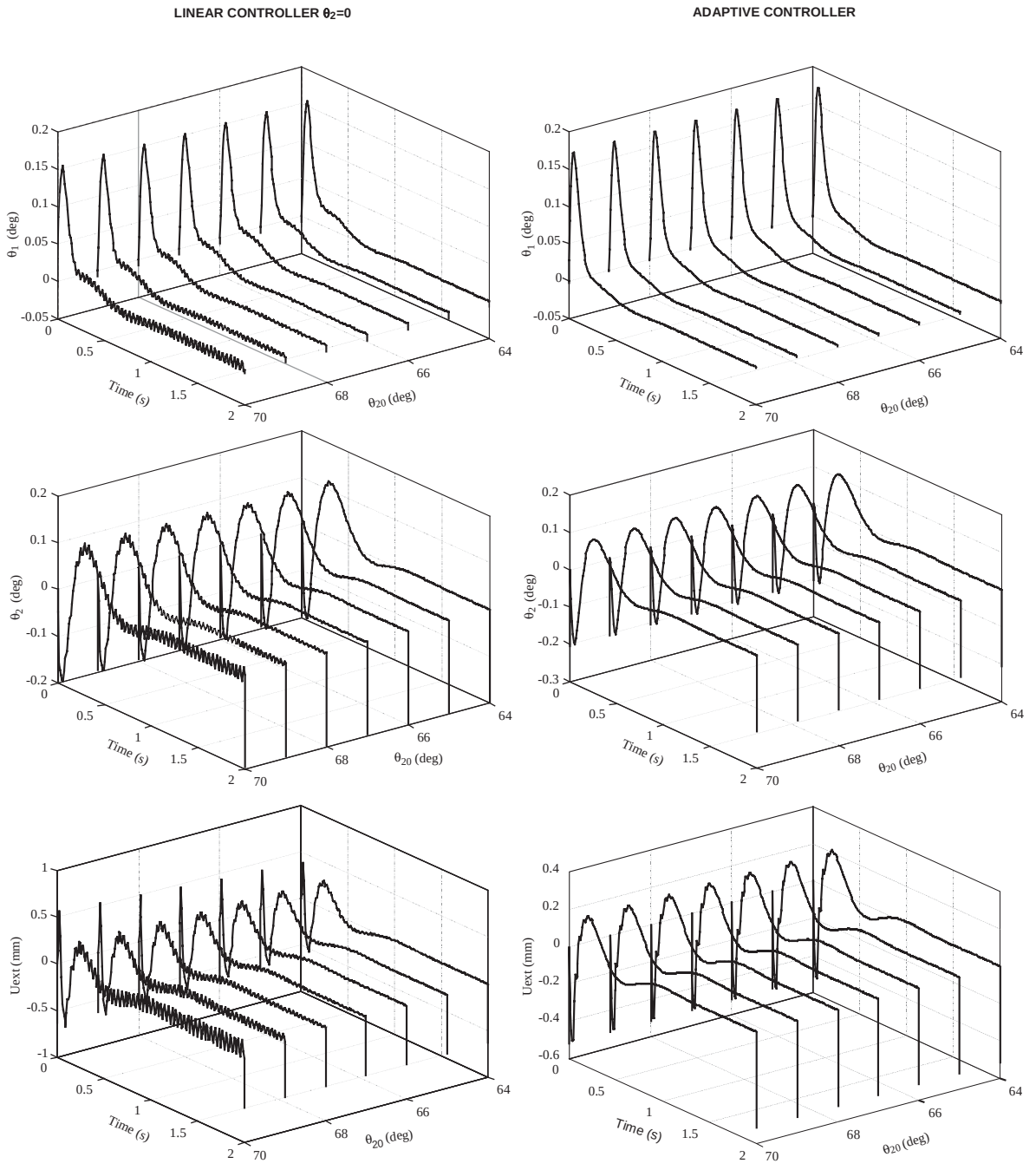

Fig. 14. Responses of the bi-articulated flexible structure for a step type disturbance generated to θ_{20} (C_{m1}: 2 NM; C_{m2}: 1 NM).

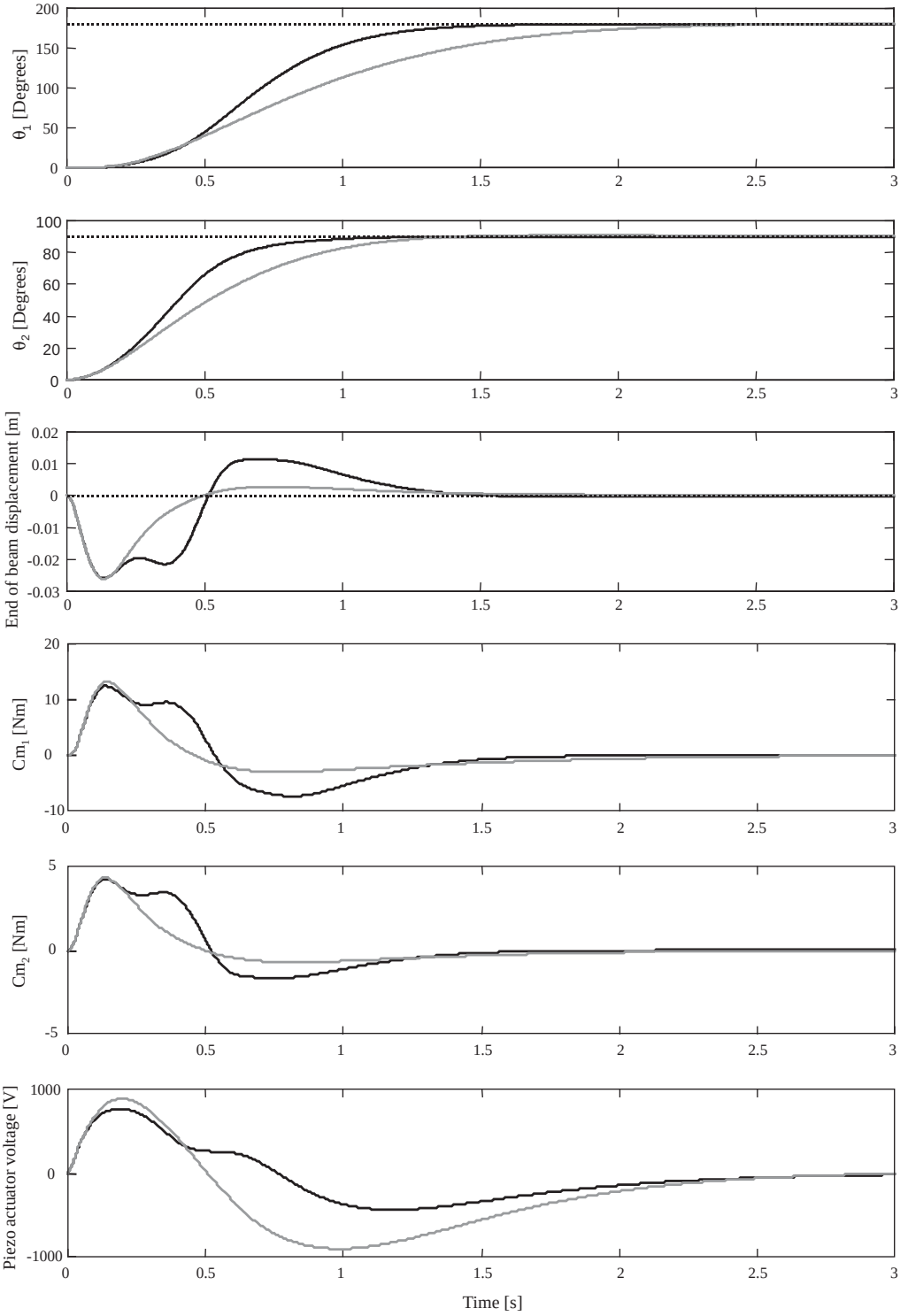

Fig. 15. Responses of the flexible bi-articulated structure—second adjustment (set points tracking $\theta_1 = 180^\circ$, $\theta_1 = 90^\circ$) (——: Adaptive, ——: Linear ($\theta = 0$), ·····: Order).

adaptive controller is maintained constant, in spite of the change in the structure's characteristics. Consequently, the responses highlight the robustness of the stability and performance of the adaptive controller.

The second adjustment aims at optimizing the time of establishment of a rotation tracking of set points ($\theta_1 = 180^\circ$, $\theta_1 = 90^\circ$) while limiting the global control to 12 Nm for the actuator generating C_{m_1}, to 5 Nm for the actuator generating C_{m_2} and to 5 V on the input of the high voltage amplifier of the piezoelectric ceramic actuators.

The tracking sweeps the various operating points chosen for the adaptive controller. Thus all the linear controllers take part in the control as the structure moves. The adjustment of the weightings of all the controllers is carried out simultaneously. They are optimized based on a temporal template of the responses and the commands.

Fig. 15 presents the responses and the commands of the controlled bi-articulated flexible structure corresponding to the linear controller established for position $\theta_2 = 0$ and to the adaptive controller. Comparison of the responses shows that the controller appreciably improves the performances of the control, in particular the rapidity, without harming precision and damping. The adaptive controller allows the use of motors 1 and 2 for longer periods at maximum power at the beginning of the movement, in order to increase rotation speed, without causing detrimental effects to the vibrations of the flexible beam via the piezoelectric actuator.

6. Conclusion

A new adaptive control method was presented in this paper to control the dynamic behavior of rigid and flexible multi-articulated structures subjected to rigid body displacements. Without control, these structures present dynamic behavior revealing considerable modification of their kinetic characteristics during motion, therefore strongly nonlinear dynamic behavior with coupling between the vibrations of the flexible parts and rigid body displacements.

Adaptive control is based on the parallel operation of LQG linear controllers whose commands are weighted by weighting functions according to changes in the geometry of the masses of these structures. To this end, the modeling of the studied structures was accurate and fitting was optimized.

In the case of regulation, the performances of this controller highlight on the one hand, the near-constant dynamic behavior of the controlled structure, in spite of the considerable changes of kinetics and, on the other hand, clearly improved performances when compared to a fixed linear controller. These performances require temporal optimization based on response and command templates. The adaptive controller proposed is thus well adapted to the rejections of disturbances in the case of coupling between rigid body displacements and vibrations. It is particularly robust in terms of stability and performance in relation to the internal changes of the structure.

In the case of a set point tracking, performances in terms of rapidity are also appreciably improved compared to those of a linear controller, while guaranteeing stability, significant damping and absolute precision without residual strains when the commands are performed. These performances require a certain amount work to achieve optimization.

The study was continued by replacing the weighting functions by a step by step progression of the controller based on information on rigid body displacements and the real-time calculation of

changes in kinetics. However, performances were not improved since there was no change in this case of the weighting matrices of the linear controllers.

The study can be extended to multi-articulated and two-dimensional structures by using the principle of this adaptive controller.

Acknowledgments

The authors particularly thank the *Région Rhone-Alpes* of France for its financial support and the scientific exchanges carried out within the framework of the project ''Modeling and Control of Complex Dynamic Systems''.

References

[1] L. Gaudiller, J. DerHagopian, Active control of flexible structures using a minimum of components, *Journal of Sound and Vibration* 193 (1996) 713–741.
[2] M. Karkoub, K. Tamma, G. Balas, Vibration control of two flexible manipulators using the μ-synthesis technique, *Journal of Vibration and Control* 5 (1999) 559–576.
[3] B.P. Nagaraj, B.S. Nataraju, Dynamics of a two-flexible system undergoing locking, mathematical modeling and comparison with experiments, *Journal of Sound and Vibration* 207 (1997) 567–589.
[4] D.A. Schoenwald, Ü. Ozgüner, On combining slewing and vibration control in flexible manipulators via singular perturbation, *Proceedings of 29th IEEE Conference on Decision and Control*, vol. 3, 1990, pp. 533–538.
[5] H.H. Yoo, R.R. Ryan, R.A. Scott, Dynamics of flexible beams undergoing overall motions, *Journal of Sound and Vibration* 181 (1995) 261–278.
[6] B. Fallahi, S. Lai, C. Venkat, A finite element formulation of a flexible slider crank mechanism using local coordinates, *Journal of Dynamic Systems, Measurement and Control* 117 (1995) 329–335.
[7] N. Azouz, M. Pascal, A. Combescure, Application de la MEF à la modélisation dynamique des robots souples, *Revue Européenne des Eléments Finis* 7 (1998) 763–791.
[8] T. Koyama, H. Asada, Design of an arm with double actuators for high speed and high accuracy manipulation, *IEEE Proceedings of the 1991 American Control Conference*, vol. 2, 1991, pp. 1435–1437.
[9] Y.C. Liu, S.M. Yang, Vibration control experiment of a slewing flexible beam, *Journal of Dynamic Systems, Measurement and Control* 117 (1995) 432–435.
[10] S.R. Waren, P.G. Voulgaris, L.A. Bergman, Robust control of a slewing beam system, *Journal of Vibration and Control* 1 (1995) 251–272.
[11] S.B. Choi, S.S. Cho, H.C. Shin, H.K. Kim, Quantitative feedback theory control of a single-link flexible manipulator featuring piezoelectric actuator and sensor, *Smart Materials and Structures* 8 (1999) 338–349.
[12] F.J. de O. Moreira, L.C.S. Goes, A. Adada Filho, $H\infty$ control of a robotic manipulator with a flexible link, *Proceedings of XV Congresso Brasileiro de Engenharia Mecânica*, Aguas de Lindóia, 1999.
[13] P.M. Chang, S. Jayasuriya, An evaluation of several controller synthesis methodologies using a rotating flexible beam as a test bed., *Journal of Dynamic Systems, Measurement, and Control* 117 (1995) 360–373.
[14] L. Meyrovitch, H. Baruh, H. Oz, A comparison of control techniques for large flexible systems, *Journal of Guidance and Control* 6 (1983) 302–310.
[15] T.T. Soong, J.C.H. Chang, Active vibration control of large flexible structures, *The Shock and Vibration Bulletin* 52 (1982) 47–54.
[16] D.C. May, S. Jayasurya, B.W. Mooring, Modeling and control of manipulator joint driven through a worm gear transmission, *Journal of Vibration and Control* 6 (1998) 85–111.
[17] A. Baz, S. Poh, P. Studer, Modified independant modal space control method for active control of flexible systems, *Proceedings of the Institution of Mechanical Engineering* 203 (1989) 103–111.

[18] J. Tani, F. Takahashi, H. Ueda, Active control of vibrating beam, *Proceedings of 10th International Symposium on Space Technology and Science*, vol. 1, 1988, 571–576.
[19] C.H. Gerhold, Active control of flexural vibrations in beams, Summer Faculty Fellowship Program, Final report NASA/ASEE, Washington, vol. 11, 1987, pp. 11–20.
[20] K.K. Denoyer, M.K. Kwak, Dynamic modeling and vibration suppression of a slewing structure utilizing piezoelectric sensors and actuators, *Journal of Sound and Vibration* 189 (1996) 13–31.
[21] H.R. Pota, T.E. Alberts, Multivariable transfer functions for a slewing piezoelectric laminate beam, *Journal of Dynamic Systems Measurement and Control* 117 (1995) 352–359.
[22] Y.H. Lin, C.L. Chu, Numerical evaluation for stability and performance of an electronic damping device for structural vibration control, *Journal of Sound and Vibration* 184 (1995) 929–933.
[23] C.F. Hung, J.T. Chiu, Vibration control of moving flexible member using piezoelectric actuators, *Journal of Engineering Mechanics* 22 (1995) 858–864.
[24] G. Celantano, R. Setola, The modelling of a flexible beam with piezoelectric plates for active vibration control, *Journal of Sound and Vibration* 223 (1999) 483–492.
[25] H.S. Tzou, R. Ye, Piezothermoelasticity and precision control of piezoelectric systems: theory and finite element analysis, *Journal of Vibration and Acoustics* 116 (1994) 489–495.
[26] C.C. Won, J.L. Sulla, D.W. Sparks, W.K. Belvin, Application of piezoelectric devices to vibration suppression, *Journal of Guidance, Control, and Dynamics* 17 (1994) 1333–1338.
[27] S. Bochard, Contrôle Actif par Composants Piezoélectriques de Structures Souples en Grands Déplacements, PhD Thesis, Institut National des Sciences Appliquées de Lyon, France, 2002.